sustainability

MDPI

Article

Autogenous Shrinkage, Strength, and Hydration Heat of Ultra-High-Strength Paste Incorporating Nano-Zirconium Dioxide

Guang-Zhu Zhang [1], Han-Seung Lee [2] and Xiao-Yong Wang [1,3,*]

[1] Department of Architectural Engineering, Kangwon National University, Chuncheon-Si 24341, Korea; zhangks@kangwon.ac.kr
[2] Department of Architectural Engineering, Hanyang University, Ansan-Si 15588, Korea; ercleehs@hanyang.ac.kr
[3] Department of Integrated Energy and Infra System, Kangwon National University, Chuncheon-Si 24341, Korea
* Correspondence: wxbrave@kangwon.ac.kr

Received: 17 September 2020; Accepted: 9 November 2020; Published: 11 November 2020

Abstract: Ultra-high-strength paste (UHSP) combined with nanomaterials has been extensively studied. However, the research on nano-ZrO_2 is limited. In this study, UHSP with various nano-ZrO_2 contents is analyzed. The motivation of this study is to clarify the effects of nano-ZrO_2 on the hydration products, strength, autogenous shrinkage, and hydration heat of UHSPs. The water-to-binder ratio (w/b) of the specimens is 0.2. The nano-ZrO_2 content is 0, 1.5, and 3 wt.%. The strength is measured at the age of 3, 7, and 28 days. The hydration heat is measured from the mixing stage to 3 days. The hydration products are analyzed by X-ray diffraction (XRD) and thermogravimetric analysis (TG). The autogenous shrinkage is measured from the mixing stage for 7 days using a new experimental device. The new experimental device can measure autogenous shrinkage, internal relative humidity, and internal temperature simultaneously. The following conclusions can be drawn based on the experimental studies: (1) Two stages were noticed in the autogenous shrinkage of UHSPs: a variable-temperature stage and a room-temperature stage. The cut-off point of these two stages occurred in roughly 1.5 days. Furthermore, in the room-temperature stage, there was a straight-line relationship between the autogenous shrinkage and internal relative humidity. (2) With the increase of the nano-ZrO_2 amount, the compressive strength at 3 days, 7 days, and 4 weeks increased. (3) With the nano-ZrO_2 increasing, the flow decreased. (4) With the nano-ZrO_2 increasing, the hydration heat increased due to the physical nucleation effect of the nano-ZrO_2. Furthermore, the nano-ZrO_2 used in this study was chemically inert and did not take part in the cement hydration reaction based on the XRD, differential thermal, and TG data. This paper is of great significance for the development of high-strength cementitious materials doped with nano-ZrO_2.

Keywords: nano-ZrO_2; ultra-high-strength paste; compressive strength; autogenous shrinkage; hydration heat

1. Introduction

Ultra-high-strength concrete is a new type of sustainable cement-based material with positive and negative effects. The positive effect includes a high compressive strength, good durability, and low CO_2 emission for unit compressive strength [1,2]. However, the negative effect is also pronounced. Because of the low water-to-binder (w/b) ratio of ultra-high-strength paste (UHSP), substantial early autogenous shrinkage is caused by the self-drying phenomenon, which is a very serious shortcoming, as it causes the concrete to demonstrate a poor volume stability and have a high risk of autogenous shrinkage

cracking [3]. The high cement content in UHSP can lead to high thermal stresses, resulting in thermal cracking in concrete structures [4]. The study of the influence of concrete mixtures on UHSP autogenous shrinkage and hydration heat is essential for the application of UHSP in practical engineering.

With the development of nanotechnology, researchers became interested in nanomaterials and applied them to the research of UHSPs. Common nanomaterials added to UHSP include nano-calcium carbonate (nano-$CaCO_3$), nano-silica (nano-SiO_2), nano-iron trioxide (nano-Fe_2O_3), and nano-titanium dioxide (nano-TiO_2), etc. Liu et al. [3] found that nano-$CaCO_3$ acted as a low reactive filler material, creating a denser microstructure in the concrete. At the same time, they also found that nano-SiO_2 reduced the pore area and accelerated the cement hydration through a pozzolanic reaction. Ghafari et al. [5] reported that nano-SiO_2 was effective in improving the interfacial transition zone between agglomerates and binding paste, and the capillary pores of ultra-high-strength concrete were reduced. Gu et al. [6] found that the addition of nano-TiO_2 refined the pore structure of ultra-high-strength concrete, improved the mechanical properties and durability of ultra-high-strength concrete, and reduced drying shrinkage.

While nanomaterials have been extensively studied in relation to UHSPs, the number of reports on nano-zirconium dioxide (nano-ZrO_2) being mixed into UHSPs as a filler is limited. Nano-ZrO_2 is a non-reactive ceramic material, which is widely used because of its high strength, excellent fracture toughness, and high corrosion resistance. Nano-ZrO_2 is even more widely used to facilitate dental tissue engineering applications due to its stable chemical bonds, which are safe and reliable for human health [7,8]. Because of its good wearability, chemical bond stability, and anti-corrosion performance, further research on the use of nano-ZrO_2 in concrete is becoming more and more valuable. The existing studies have focused to a greater extent on the effect of nano-ZrO_2 addition on the microstructure, electrical properties, and mechanical properties of concrete. Han et al. [9] studied the mechanical qualities of concrete combined with nano-ZrO_2 and found that 3 wt.% nano-ZrO_2 improved the 28-day compressive, flexural, and splitting strengths by about 16.3%, 36.6%, and 16.18%, respectively. Ruan et al. [10] studied the result of water curing and heat curing in relation to the qualities of concrete combined with nano-ZrO_2. The experimental results show that the heat curing method is more significant for nano-ZrO_2 in terms of improving the densification of the substrate, compared to water curing. Trejo-Arroyo et al. [11] synthesized nano-ZrO_2 particles by co-precipitation and by adding such particles to the mortars, and they observed the microscopic development and physical and mechanical properties of mortars. A series of data revealed that nano-ZrO_2 was able to make the mortar structure denser and increased the compressive strength. Yuan et al. [12] studied the effect of nano-ZrO_2 on the thermal properties of concrete. The results of the experimental data on thermal conductivity, volumetric heat capacity, and expansion coefficient showed that nano-ZrO_2 can improve the thermal conductivity and bulk heat capacity of concrete, which is very favorable for high-heat storage material applications. While there are studies in the literature that revealed the effect of nano-ZrO_2 on various properties of concrete, these studies are still scarce. First, some nanomaterials, such as nano-$CaCO_3$ [13], have a certain degree of reactivity to cement hydration. Whether nano-ZrO_2 is reactive to the cement matrix requires further investigation. Second, some researchers [9,12] have carried out research regarding the effect of nano-ZrO_2 on UHSPs, but the research is limited, especially in relation to the influence of nano-ZrO_2 on the autogenous shrinkage of UHSP. The influence of nano-ZrO_2 on the trend of autogenous shrinkages of UHSP has not been investigated. Finally, the autogenous shrinkage of cast-in-place concrete is one of the influencing factors that cannot be ignored. For the initial stage of cement hydration, the internal temperature increase, autogenous shrinkage, and internal relative humidity are coupled together, and for this reason, it is necessary to conduct a systematic study.

This study aimed to investigate the effect of nano-ZrO_2 on the autogenous shrinkage, hydration heat, and strength of UHSP. The mechanisms by which nano-ZrO_2 affects the autogenous shrinkage and hydration kinetics of UHSP were clarified using isothermal calorimetry, autogenous shrinkage data, X-ray diffraction, compressive strength, and differential thermal and thermogravimetric analyses. This paper therefore fills a research gap in the existing literature.

The original points and discoveries of this paper are summarized as follows: (1) The mechanism of the development of the autogenous shrinkage of UHSPs mixed with nano-ZrO_2 is investigated. (2) The trend of the internal relative humidity in UHSPs was divided into two stages, with the cut-off point occurring at 1.5 d. In the first stage (the V stage), the internal relative humidity underwent a decrease early on and then an increase to the maximum with time. In the second stage (the R stage), the internal relative humidity decreased continuously with time. (3) The effect of the addition of nano-ZrO_2 on the hydration of UHSPs was analyzed. It was proved that the nano-ZrO_2 in this study was chemically inert and did not take part in the reaction of cement hydration. (4) The total heat release of UHSPs increased with increasing amounts of nano-ZrO_2. The nano-ZrO_2 has a physical nucleation effect, resulting in a reduced setting time.

2. Materials and Methods

2.1. Materials and Specimen Preparation

The primary purpose of this paper is to investigate the effects of nano-ZrO_2 (nZr) on the hydration products, strength, hydration heat, and autogenous shrinkage of cement-based materials (cement pastes). Aggregate makes XRD and TG experiments difficult to perform, so paste specimens were used for this study. Ordinary Portland cement (OPC) and nano-ZrO_2 (nZr) were utilized as binders for that UHSP mix design. The OPC was obtained from Sungshin Cement Co., Ltd. (Seoul, Korea), and the nZr was obtained from Ningbo Jinlei Nano Mstar Technology, Ltd. (Ningbo, China). The average particle size of the nZr was 50 nm, and the specific surface area was 80 m^2/g. Figure 1 shows a scanning electron microscope image of nZr. The chemical compositions of OPC and nZr are listed in Table 1. The physical properties of cement are listed in Table 2. The superplasticizer was a polycarboxylate (PCE) superplasticizer, and it was supplied by Dongnam Co., Ltd. (Seoul, Korea).

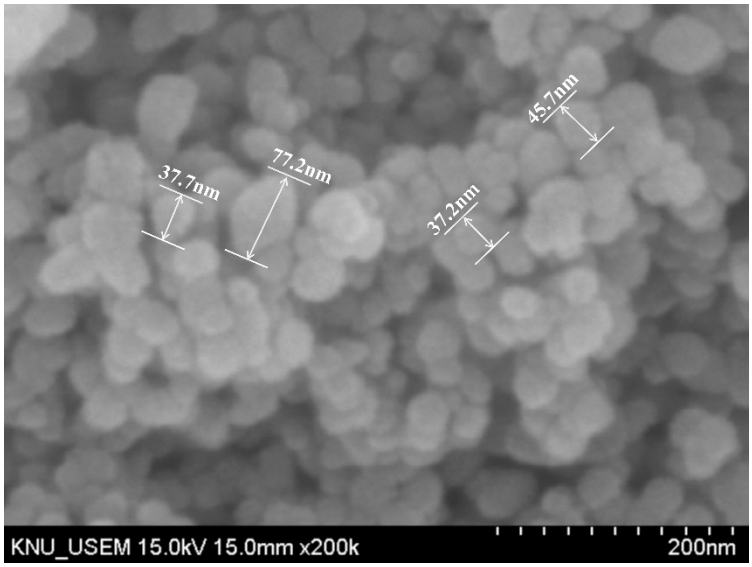

Figure 1. Morphology of raw nano-ZrO_2.

Table 1. Compositions (wt.%) of binders.

	SiO_2	ZrO_2	CaO	Fe_2O_3	SO_3	MgO	ZnO	Al_2O_3	K_2O	Loss
Cement	21.95	-	61.28	2.43	2.84	2.87	0.11	6.19	1.78	0.54
Nano-ZrO_2	-	99.90	-		-		-		-	-

Table 2. Physical properties of Portland cement.

Density (kg/cm^3)	Specific Surface Area (m^2/kg)	Setting Time (Min)		Compressive Strength (MPa)	
		Initial	Final	3 d	28 d
3.14	345	205	295	29.5	58.9

The mix proportion design of UHSP is shown in Table 3. First, all powders (cement and nano-ZrO_2) were put into a mortar mixer and mixed at a low spend for 30 s. Then, water, combined with the superplasticizers, was mixed into the powders, and stirred at a low speed for just 2 min. Then, the blending was stopped for 30 s, and the paste was hung on the inner wall of the mixing bowl and the mixing paddle. Finally, the paste was stirred at a high speed for 3 min. All mixing was carried out at room temperature and maintained at 20 ± 1 °C. The aim of this paper was to clarify the effect of nZr on various properties of UHSP. Because the particle size of nZr is pretty small, it is difficult to disperse nZr in water. In order to ensure a good dispersion, the amount of nanomaterials added is usually less than 5% [12]. The 10–20 wt.% addition is difficult to implement. The control group was named nZr0. The composite pastes were prepared with cement and nZr at nZr-replacement amounts of 1.5 and 3 wt.%, denoted as nZr1.5 and nZr3, respectively. The polycarboxylate superplasticizer amount was 0.8 wt.%, and it was added to all mixtures. The w/b ratio of UHSP is usually between 0.15 and 0.25. The w/b ratio of the specimens in this study was equal to 0.2. This paper investigates the effect of the nZr substitution rate on UHSP, and the w/b ratio was constant. In our future study, the effect of the w/b ratio on UHSP will be studied.

Table 3. Mix proportion design of specimens.

Number	Binders				Water	Superplasticizer	
	Cement		nano-ZrO_2				
	%	kg/m^3	%	kg/m^3	kg/m^3	%	kg/m^3
nZr0	100	1906	0	0	381	0.8	15
nZr1.5	98.5	1876	1.5	29	381	0.8	15
nZr3	97	1845	3	58	381	0.8	15

Target values, such as workability and compressive strength, are important factors for the mixture design of UHSP. This study clarifies the effect of nZr on such things as workability and compressive strength. The experimental results in this study are useful for the mixture design of UHSP with nZr. In the future study, we will study the mix design in consideration of the target values of workability and compressive strength.

2.2. Experimental Program

2.2.1. Workability

The mini-slump flow measurement of UHSP was carried out according to ASTM C 1437 [14]. After mixing, the fresh UHSP mixture was poured into a tapered mold. After the conical die was removed, the average of the two diameters perpendicular to each other as the minimum slump of the UHSP was recorded.

2.2.2. Isothermal Calorimetry

An isothermal calorimeter was used to investigate the effect of nZr on the hydration rate of UHSP. Samples were prepared according to the above mix design. The sample consisted of cement materials, water, and PCE. After a mortar mixer mixed the above components, approximately 5 g of paste was weighed and then injected into a glass bottle through a syringe. The whole process and the measurement of the isothermal calorimetry experiment were controlled at 20 °C.

The determination of the setting time is usually determined using the Vicat needle method. In this study, the isothermal calorimetry method was used. Hu et al. [15] used the Vicat needle and isothermal calorimetry methods to measure the setting times. Hu et al. found a linear relationship between the isothermal calorimetry and Vicat needle methods, and the basic trend of the two methods was similar. Therefore, we used the isothermal calorimetry method to determine the setting time and clarify the effect of nZr on setting times.

2.2.3. Autogenous Shrinkage, Internal Temperature, and Relative Humidity

A corrugated tube method was adopted by the researchers to measure the autogenous shrinkage of cement pastes and mortars based on ASTM C1698-09 [16]. In this study, the autogenous shrinkage device has been improved based on the ASTM C1698-09. The original ASTM C1698-09 experimental device can only measure changes in autogenous shrinkage. It is well known that internal relative humidity (IRH) and internal temperature (IT) are important influential factors in autogenous shrinkage (AS). Therefore, we have made some improvements to the original device. The improved device in this study can measure the internal relative humidity, internal temperature, and autogenous shrinkage simultaneously.

Figure 2 shows a drawing of the design of the improved autogenous shrinkage measuring device. By inserting a temperature and humidity transmitter in the specimen center, the new experimental device can measure the AS, IT, and IRH data of specimens during the hydration reaction. The paste was poured into a corrugated plastic tube, and then the corrugated plastic tube was placed on a steel support. A magnet, pre-installed on one end of the corrugated plastic tube plug, was adsorbed to one end of the steel support, and another plug was left without setting constraints so that it could move freely. The linear variable differential transducer (LVDT) measured the length change of the specimens. The temperature and humidity transmitter, covered with a PVC tube, was inserted in the center of the specimen to measure the IRH and IT of the UHSPs. The LVDT and temperature and humidity transmitters were connected to a computer, and data on the microstrain, internal relative humidity, and internal temperature were collected every 10 min. The entire setup was placed in a thermostat (20 ± 1 °C) for the test at 7 days. The accuracy of the IRH and IT of the transmitter was ±0.8% RH and ±0.1 °C, respectively. The whole experimental process was operated at 20 ± 1 °C.

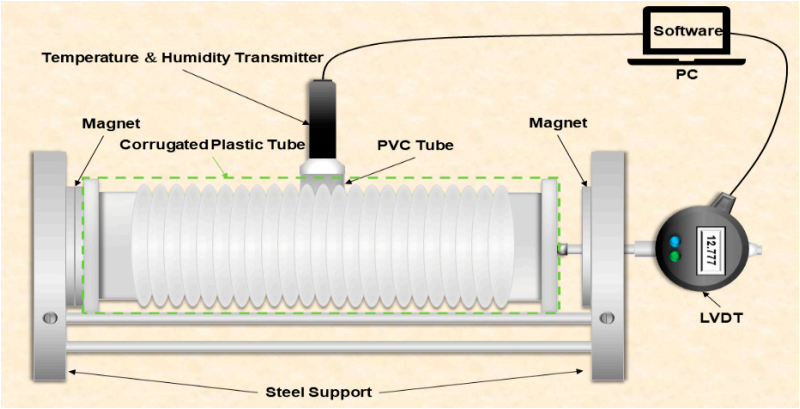

Figure 2. Drawing of the design of the improved experimental measuring device.

2.2.4. X-ray Diffraction

X-ray diffraction (XRD) was conducted to look at the crystalline phases within the examples cast at 4 weeks old. XRD was transported out using a PANalytical X'Pert-pro MPD diffractometer, with Cu Kα radiation, one step size of 0.1°, and a 2θ selection of 10–75°.

2.2.5. Compressive Strength Test

The examples for the strength test were tested according to the ASTM C349-18 standard [17]. The size of the specimens was 40 × 40 × 160 mm. The specimens were removed from the molds after curing for 24 h in a standard curing chamber (20 ± 1 °C). The examples were sealed using polyethylene film and stored inside a constant temperature chamber at 20 °C for 3 days, 7 days, and 4 weeks. Three specimens were subjected to three-point bending, resulting in six samples that were employed to measure the compressive strength. For the test, the load rate was maintained at 1.5 N/(mm^2·s). The average value of the six specimens was used as the compressive strength. The main objective of this paper was to analyze the effect of nano-ZrO_2 on the compressive strength, autogenous shrinkage, hydration heat, and hydration products of UHSP. The flexural properties were not the main focus of this study. In future studies, we will investigate the effect of nano-ZrO_2 on the flexural strength and other properties of concrete.

2.2.6. Differential Thermal and Thermogravimetric Analysis (DTA-TG)

The DTA-TG experiment was performed based on the ASTM E1131 standard. The equipment used by SDT Q600 was provided by TA Instruments (New Castle, Germany). The balance sensitivity of the equipment was 0.1 µg. The dynamic heating ramp varied between 40 and 1050 °C. The heating rate was 15 °C/min, and the pans used were made of ceramic. The test space of the sample was filled with N_2, and the N_2 filling rate was 100 mL/min. All samples were taken from a pre-ground sample of approximately 30 mg. Table 4 shows the number of specimens and the experiment precision for every experiment.

Table 4. Number of specimens and experiment precision for every experiment.

Test	Numbers of Specimen for Each Group	Experiment Precision
Mini-slump flow	2	1 mm
Isothermal calorimetry	1	±20 µW
Autogenous shrinkage	1	0.001 µm/m
Internal temperature	1	±0.1 °C
Internal relative humidity	1	±0.5% RH
X-ray diffraction	1	λ = 1.5406 Å 2 θ = 0.013°
Compressive strength	6	Within ±0.05% of the indicated load
Differential thermal and thermogravimetric analysis	1	0.1 µg

3. Results

3.1. Slump Flow

The flow results of fresh UHSP mixes are shown in Figure 3. It is noteworthy that with the addition of nZr, the flow of the UHSPs showed a decline. The flow of nZr0, nZr1.5, and nZr3 were 360, 332.5, and 257.5 mm, respectively. This behavior is mainly due to the fact that the presence of nanoparticles reduces the amount of lubricating water available in the intergranular voids, thus increasing the yield stress of UHSPs mixed with nZr [18]. Different nanomaterials have different surface properties. The average specific surface areas of nano-SiO_2 and nano-TiO_2 are usually 600 and 50 m^2/g, respectively. The specific surface area of the nano-ZrO_2 used in this study was 80 m^2/g. The flow of concrete with the addition of nanomaterials was reduced due to the high specific surface area of the nanomaterials [19]. Since the specific surface area of nZr is much larger than that of cement, the dispersion of nZr is the main reason for the high flowability of UHSP. Since the superplasticizers (PCE type) used in this study improved the bonding between nZr and the cement matrix and, at the same time, attached functional groups (-COOH) to the nZr surface to reduce the Van der Waals forces, it resulted in a better dispersion effect and reduced the aggregation [20]. In addition, more water also reduces aggregation. The flow of

UHSP also relates to the point of zero charge (pzc) [21,22]. The pzc for ZrO_2 ranges from 3.2 to 4.2. The pH of the concrete in this study was about 12.8 [23]. The pH value of concrete is above the pzc for ZrO_2 ranges, and the surface charge would be negative [24]. In summary, the flow of UHSP showed a decreasing trend with the increase of the nano-ZrO_2 amount.

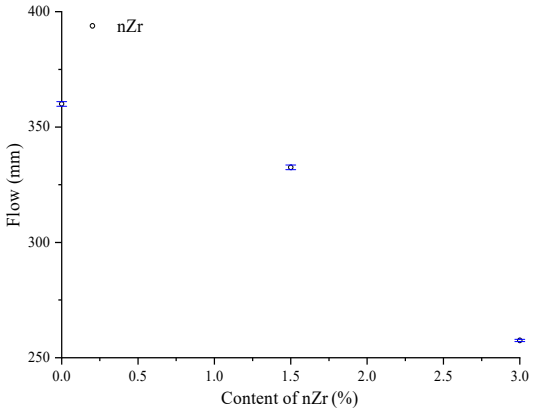

Figure 3. The relationship between the flow and nano-ZrO_2 amount.

3.2. Isothermal Calorimetry

Figure 4 shows the isothermal calorimetry results of the UHSPs with different nZr amounts and without nZr. Since the cement pastes were prepared outside the calorimeter, the first peak caused by the rapid hydration of tricalcium aluminate (C_3A) was not completely captured.

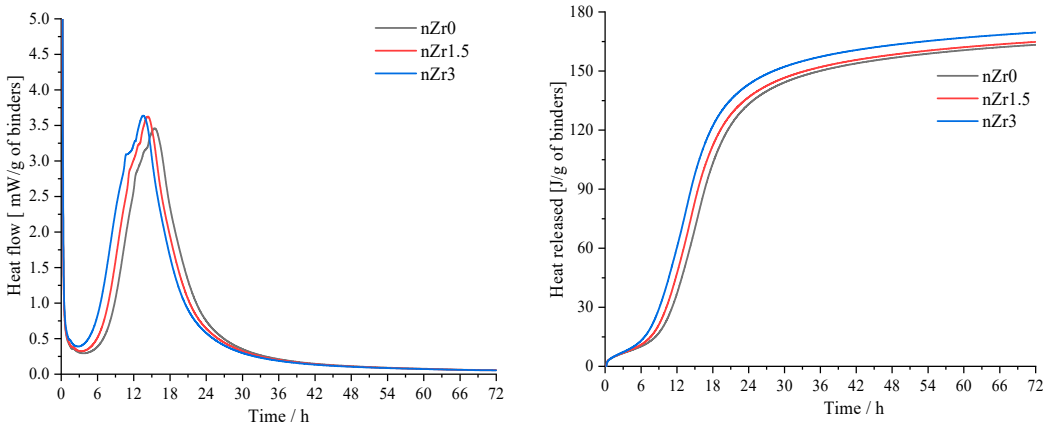

(**a**) Heat flow rate (**b**) Total heat of hydration

Figure 4. Isothermal calorimetry data for the heat flow rate (**a**) and total hydration heat (**b**) of the ultra-high-strength pastes (UHSPs) with different nano-ZrO_2 (nZr) amounts.

Figure 4a shows the relationship between the binder hydration reaction and heat flow. Compared with the heat flow of nZr0, the nZr addition increased the height of the main heat flow peak and shortened its appearance time. However, regardless of the nZr content, the main peaks of nZr1.5 and nZr3 show similar intensities. As the nZr amount increased, the main peak appeared earlier. The main peaks of the UHSP heat flows appeared in the order of nZr3 > nZr1.5 > nZr0. Figure 4b shows the curve of the heat accumulation of the UHSPs for the 72 h hydration reaction. The nZr addition resulted in a greater cumulative heat release in the UHSP. The final heat release values of nZr3, nZr1.5, and nZr0 were 169.58, 164.81, and 163.08 J/g, respectively. The main reason for this behavior is that nZr has a higher specific surface area. By adding more surface area for the formation of hydration productions, more nucleation sites are provided [25]. Meng et al. [26] reported the hydration heat results of Ultra

high-performance concrete containing graphite nanoplatelets and found that the total hydration heat increased with the increasing graphite nanoplatelet content. Compared with the hydration heat results in this study, both experiments have similar development trends.

The setting time was determined according to the first derivative of the hydration heat from the isothermal calorimetry method [15]. The time of the initial setting was determined according to the first derivative curve reaching its maximum value, and the increase in the value of the first derivative was the highest at this time. Following the time of the initial setting, the value of the first derivative started to decrease. The time when the first derivative dropped to zero was understood to be the time of the final setting. The rate of hydration arrived at its greatest value at that moment.

Figure 5 shows the curve obtained from the first derivative of the heat flow. By definition, the times of the initial setting of nZr0, nZr1.5, and nZr3 were 10.3, 9.3, and 8.15 h, respectively. The times of the final setting of nZr0, nZr1.5, and nZr3 were 15.38, 14.26, and 13.53 h, respectively. Through the derived data, it can be observed that the setting time was reduced with the addition of nZr to the UHSPs. This behavior occurs because the nZr addition provides more nucleation sites for the formation of hydration productions [27]. In this study, the setting time of UHSP was higher than that of previous similar studies [28,29]. The occurrence of this phenomenon is mainly related to the test method and concrete mix ratio. For concrete mixtures, Zhang et al. [30] reported that polycarboxylate superplasticizers can slow down the hydration of cement, resulting in an increase of the setting time. This behavior is mainly due to the surface dissolution, and product nucleation sites are inhibited by the adsorption of polycarboxylate molecules, leading to a delay of the hydration kinetics [31]. Summarily, due to the combined effect of the testing method and superplasticizer addition, the setting time of ultra-high-strength concrete in this study was significantly high (approximately 10 h).

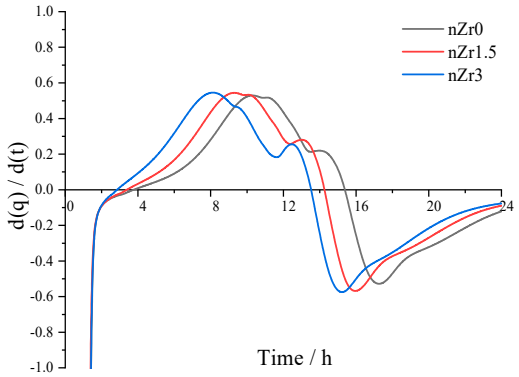

Figure 5. A curve of the first derivative of hydration heat (d(q)/d(t)).

3.3. Development of Autogenous Shrinkage, Internal Temperature, and Internal Relative Humidity

3.3.1. Autogenous Shrinkage

Figure 6 shows the autogenous shrinkage strain of the UHSPs with different nZr amounts for 7 curing days. Firstly, the AS rate of all specimens was higher from time zero (time of the final setting) to 3 days. After 3 days, the AS rate of nZr0 and nZr1.5 decreased, and the variation trend was similar. The slope of the AS-time curve of nZr3 showed a decreasing trend as the age increased. In addition, the slope of nZr3 was higher than that of nZr0 and nZr1.5. At 7 days of age, the AS strain of nZr0, nZr1.5, and nZr3 reached −1158, −1222, and −1739 μm/m, respectively. The total AS strain increased as the nZr amount increased. The higher the amount of nZr, the more pronounced this phenomenon. This behavior was mainly caused by the addition of the nanoparticles, which worked as a filler to improve the UHSPs' microstructure, resulting in a fine microstructure and a higher shrinkage [32]. Tafesse et al. [33] measured autogenous shrinkages of pastes with different carbon nanotube amounts (0.3 wt.% and 0.6 wt.%). It was found that the autogenous shrinkage strain of the high-strength pastes increased with the increasing carbon nanotube amount. The results in this study are similar to those

of the experiments of Tafesse et al. All autogenous shrinkage strains in both experiments exceeded 1000 μm/m at 7 days of age, and both experiments exhibited a high autogenous shrinkage behavior after the addition of nZr or carbon nanotubes. Secondly, compared with nZr0, the AS of nZr1.5 and nZr3 increased by 5.53% and 50.17%, respectively. The relationship between the AS and nZr amount was non-linear, and the AS increased when the nZr amount was increased to 3%.

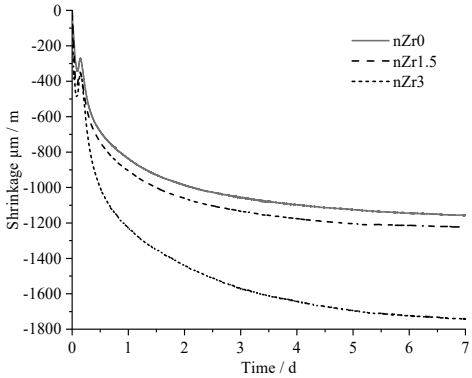

Figure 6. Autogenous shrinkage of nZr0, nZr1.5, and nZr3 at 7 days of age.

3.3.2. Development of Properties

Figures 7–9 show the experimental results of the AS, IRH, and IT of the UHSPs with different nZr amounts. In analyzing the information on IRH, it might be observed the event trend of autogenous shrinkage is split up into two stages: a variable-temperature stage (V stage) and a room-temperature stage (R stage). The cut-off point of the stages occurred in roughly 1.5 days.

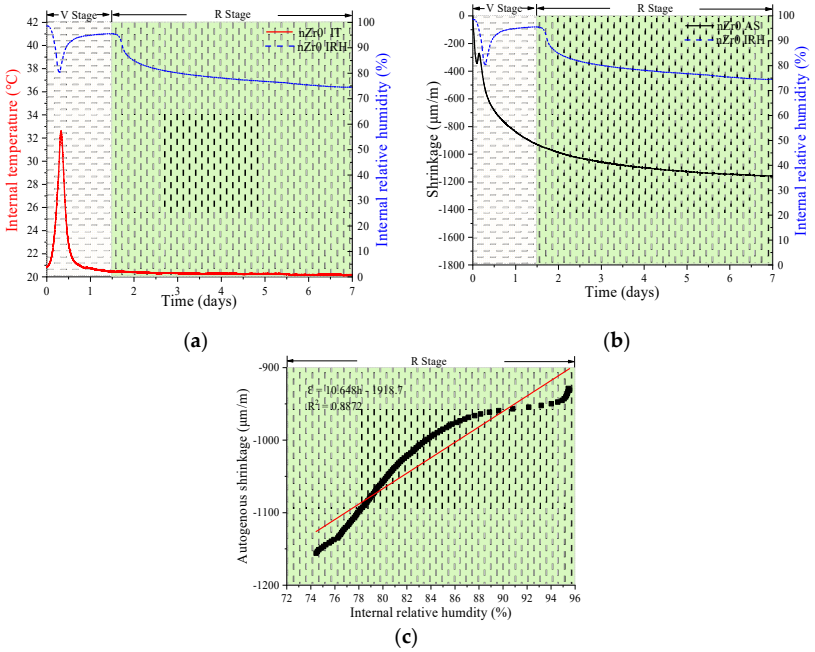

Figure 7. Relationship between various properties of the nZr0: internal temperature (IT) and internal relative humidity (IRH) (**a**); autogenous shrinkage (AS) and IRH (**b**); and the linear regression results of IRH and AS in the R stage (**c**).

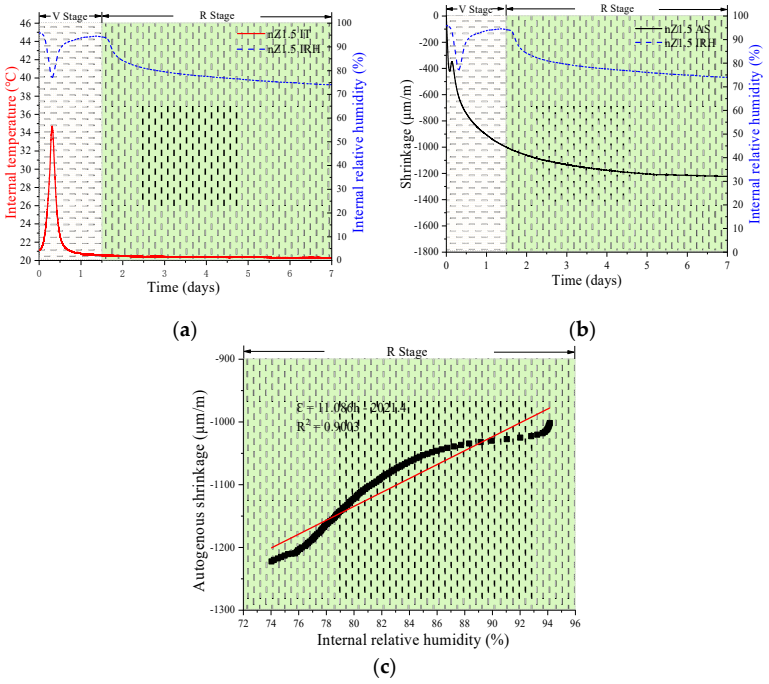

Figure 8. Relationship between various properties of the nZr1.5: IT and IRH (**a**); AS and IRH (**b**); and the linear regression results of IRH and AS in the R stage (**c**).

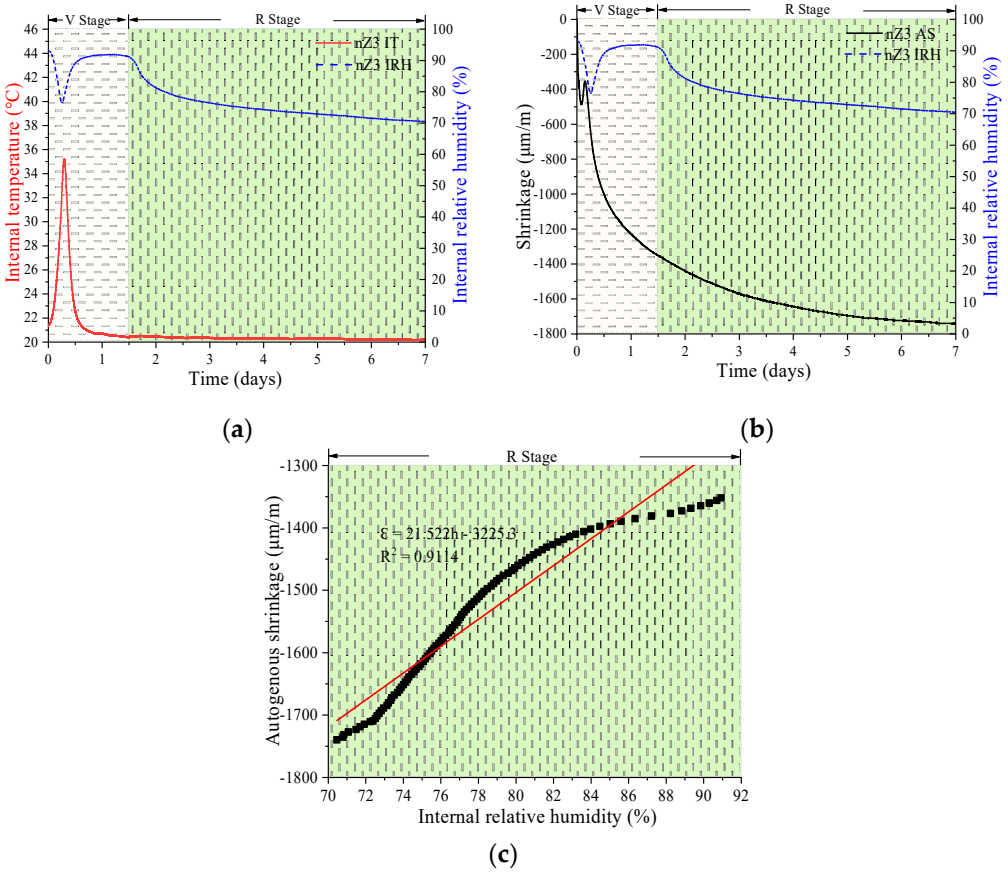

Figure 9. Relationship between various properties of the nZr3: IT and IRH (**a**); AS and IRH (**b**); and the linear regression results of IRH and AS in the R stage (**c**).

Firstly, in the V stage, the IT of all specimens increased and then decreased. The maximum IT values for the nZr0, nZr1.5, and nZr3 specimens were 32.6, 34.71, and 35.19 °C, respectively. In Figure 4a, it can be clearly observed that the hydration rate increased due to the nZr amount increasing, before the cut-off point (1.5 days). The results of the three experiments showed similar trends. Secondly, in the V stage, an interesting phenomenon was observed; the IRH curve peaks of all specimens firstly decreased and then increased. At the same time, we also found that the time when the lowest point of the IRH peak appeared corresponds to the time when the maximum IT value appeared. The reason for this phenomenon was that the continuous hydration reaction reduced the IRH of the specimen. In addition, the binder hydration reaction also raised the IT, and the water in the ink-bottle space was released and redistributed in the form of condensed water, resulting in the IRH increasing. Therefore, it was the combination of the two factors that made the IRH curve firstly decrease and then increase. Finally, in the R stage (after 1.5 days), the IRH continued to decrease. This phenomenon was mainly due to the continuous hydration reaction that consumed part of the water and caused the IRH to fall continuously. The final IRH values of nZr0, nZr1.5, and nZr3 at 7 days of age were 74.56%, 74.09%, and 70.49%, respectively. The changing trend of IRH was similar to the ASs of nZr0, nZr1.5, and nZr3, which were −1158, −1222, and −1739 μm/m, respectively. The effect of nZr on the autogenous shrinkage of UHSP did not increase proportionally to the increase in the nZr amount. In addition, as shown in Figures 7c, 8c and 9c, the AS and IRH had a linear relationship. In the R stage, the IT of the specimen was a constant temperature, so self-drying caused the autogenous shrinkage. In a recent study, Bentz et al. [34] found a linear relationship between the IRH decreasing and the AS increasing.

3.4. X-ray Diffraction

Figure 10 shows the XRD patterns of the UHSPs at the curing age of 4 weeks. The calcium hydroxide (CH) could be roughly confirmed through the intensity change from the primary diffraction CH peak, like the (001) and (101) crystalline planes (d = 0.490 and 0.263 nm, respectively).

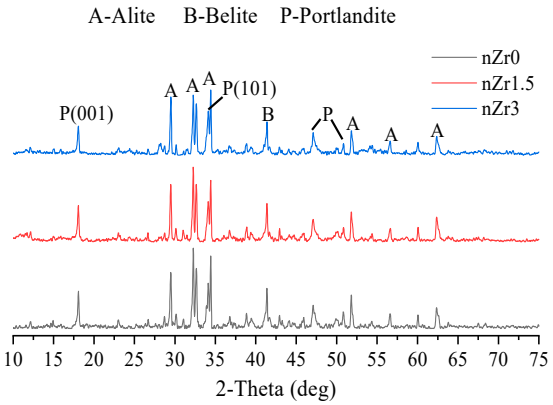

Figure 10. XRD data on UHSPs at the curing age of 4 weeks.

From the XRD data, it can be found that the height of the CH peak was almost the same. Moreover, there were no new production peaks due to the nano-ZrO_2 addition. No new hydration products were found in the XRD qualitative analysis.

On the basis of the measured experimental data, the peak intensity of the CH crystal on the (001) and (101) faces could be obtained. The CH orientation was defined as *R* [35], which was obtained from Equation (1).

$$R = 1.35I_{(001)}/I_{(101)} \quad (1)$$

where $I_{(001)}$ and $I_{(101)}$ are the peak intensities of the CH crystal on the (001) and (101) faces, respectively.

Table 5 shows the calculated results of the CH orientations. The calculation results show that with the increase in the amount of nZr, the internal CH orientation degree of the UHSPs decreased, resulting

in the compressive strength increasing [36]. In this study, based on the XRD results, the CH orientation degree was calculated. The CH orientation degree decreased, resulting in the concrete microstructure being more dense. Zhang et al. [37] demonstrated that when the CH orientation degree was reduced, the strength was enhanced, and the concrete matrix exhibited a denser microstructure. Therefore, in this study, a denser microstructure was indirectly demonstrated by the measured decrease in the CH orientation degree [38].

Table 5. Diffraction intensity and orientation of calcium hydroxide (CH) at the age of 4 weeks.

Samples	(001)CH	(101)CH	CH Orientation
nZr0	286	340	1.13
nZr1.5	281	366	1.04
nZr3	240	338	0.96

3.5. Thermogravimetry

Figure 11 shows the DTA-TG curves of nZr0, nZr1.5, and nZr3 at 4 weeks of age. The mass loss step at 400 and 500 °C is due to the portlandite ($Ca(OH)_2$) decomposition. The CH_1 represents the $Ca(OH)_2$ associated with the portlandite decomposition. The decomposition peak of calcium carbonate occurs at 600–800 °C. According to our experiments and previous references [39,40], the calcium carbonate decomposition is mainly concentrated in the range of 600–750 °C, with a portion occurring in the range of 750–800 °C. The cement hydration produces CH, and during the preparation of the TG samples, some of the CH was carbonated to form calcium carbonate ($CaCO_3$). This portion of $CaCO_3$ is derived from the CH in the hydration product, so this portion of CH should be included in calculating the total CH mass. The peak of the $CaCO_3$ decomposition found in this study is similar to that found in other researchers' studies [41]. The CH2 represents the $Ca(OH)_2$ associated with the decomposition of calcium carbonate. The mass of CH_1 and CH2 was calculated according to [42]. The CH_{total} represents the total CH of CH_1 and CH2.

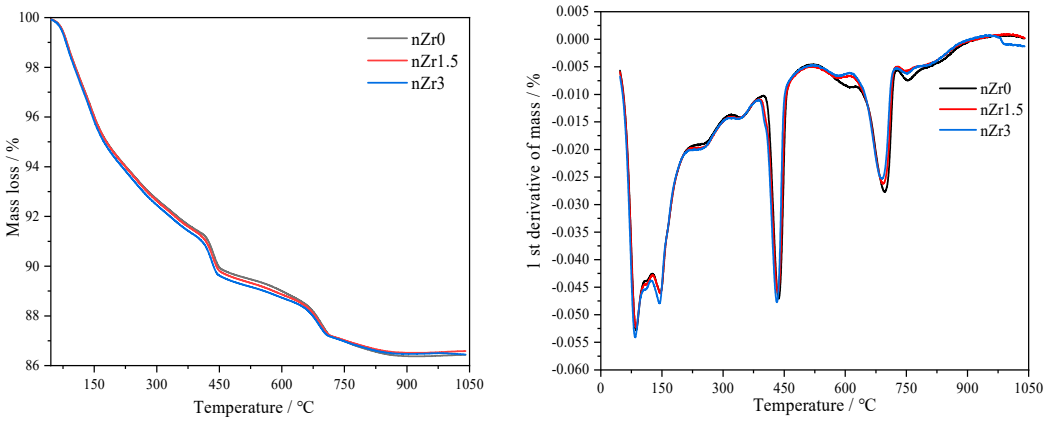

(**a**) (**b**)

Figure 11. Thermogravimetric (TG) diagram (**a**) and differential thermogravimetry (DTG) diagram (**b**) for nZr0, nZr1.5, and nZr3 at the curing age of 4 weeks.

The mass of CH_1 was obtained from Equation (2).

$$m_{CH_1} = WL_{Ca(OH)_2} \times \frac{m_{Ca(OH)_2}}{m_{H_2O}} = WL_{Ca(OH)_2} \times \frac{74}{18} \quad (2)$$

where m_{CH_1} represents the mass of CH_1, $WL_{Ca(OH)_2}$ represents the weight loss of $Ca(OH)_2$, and $m_{Ca(OH)_2}$ and m_{H_2O} represent the molecular masses of portlandite and water, which are 74 g/mol and 18 g/mol, respectively.

The mass of CH2, was obtained according to Equation (3).

$$m_{CH_2} = WL_{CaCO_3} \times \frac{m_{Ca(OH)_2}}{m_{CO_2}} = WL_{CaCO_3} \times \frac{74}{44} \quad (3)$$

where m_{CH_2} represents the mass of CH_2, WL_{CaCO_3} represents the weight loss of $CaCO_3$, and m_{CO_2} represents the molecular mass of CO_2, which is 44 g/mol.

The mass of CH_{total} was obtained from Equation (4).

$$m_{CH_{total}} = m_{CH_1} + m_{CH_2} \quad (4)$$

where $m_{CH_{total}}$ represents the total mass of CH_1 and CH_2.

Table 6 shows the CH_1, CH2, and CH_{total} amounts, normalized per gram of binder of UHSP. The CH amount depends on the CH generated by binder hydration. It was found, from the calculation results, that the amount of CH_{total} is almost the same as the nZr addition. Therefore, nano-ZrO_2 is not like other nanomaterials, such as nano-silica [43,44], which have a significant effect on cement hydration. In this study, XRD qualitative analysis was combined with TG quantitative analysis. XRD qualitative analysis can determine the type of hydration product, and TG quantitative analysis can determine the amount of CH. From the XRD qualitative analysis, no new hydration products were found. From the TG quantitative analysis, the amount of CH from all samples was found to be almost the same. Therefore, combining the two analytical methods, it was found that nZr is chemically inert and did not take part in the cement hydration reaction. It is possible to come to the same conclusion using XRD and TG curves exclusively. In this study, we quantified the total CH mass to indicate the degree of hydration of cement. Typically, when 1 g of cement hydrates, 0.25 g (0.2–0.3 g in [45]) of CH will be produced. As shown in Table 6, at the age of 28 days, the CH produced for one gram of cement is about 0.12 g. Hence, the degree of hydration is about 0.48 = 0.12/0.25, which is very low. Similar to our study, other researchers also found that the degree of hydration in UHSP is very low [46].

Table 6. Mass of CH_1, CH2, and CH_{total} per gram of cement at the curing age of 4 weeks.

Sample Codes	nZr0	nZr1.5	nZr3
m_{CH_1} (g)	0.0862	0.0882	0.0876
m_{CH_2} (g)	0.0365	0.0336	0.0319
$m_{CH_{total}}$ (g)	0.1227	0.1218	0.1195

3.6. Compressive Strength

Figure 12 shows the strength of the UHSPs at the curing age of 3 days, 7 days, and 4 weeks. The specimen employed for this test was cement paste with a side period of 40 × 40 × 160 mm. It was discovered that irrespective of the curing age, the compressive strength was elevated because the nZr amount was elevated. The primary reason behind this phenomenon is that with a growing amount of nZr, the interior CH orientation amount of the UHSPs decreased. The trends in compressive strength and autogenous shrinkage at 7 days of age have been compared. Compared to the nZr0, when the nZr addition amount was 1.5 wt.%, the increase in the autogenous shrinkage strain was marginal, and the compressive strength increased by 1.0%. When the nZr amount was 3 wt.%, the autogenous shrinkage strain increased significantly, and the compressive strength increased by 13.2%. The trend of compressive strength was similar to the trend of autogenous shrinkage at 7 days of age. Compared with the 28-day compressive strength of nZr0 (91.9 MPa), the 28-day compressive strength of nZr1.5 (98.8 MPa) and nZr3 (105.0 MPa) increased by 7.5% and 14.27%, respectively.

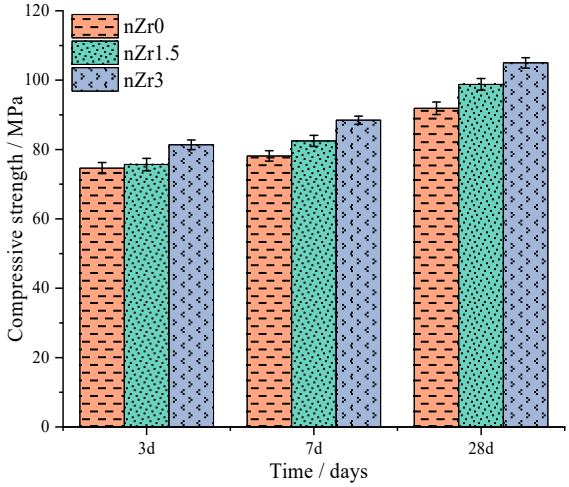

Figure 12. Compressive strength of nZr0, nZr1.5, and nZr3 at the curing age of 3 days, 7 days, and four weeks.

Figure 13 shows the connection between strength and the cumulative heat of hydration at three days of age for the UHSPs. Three measurement points are not sufficient for the linear analysis. In this study, we aimed to observe the basic trend between 3 d compressive strength and hydration heat. The strength and cumulative heat were built with a straight line relationship. The hydration heat originated from the hydration of binders, and the strength originated from the depositing of reaction products.

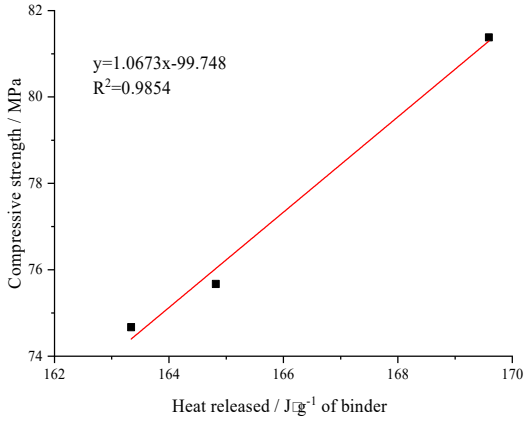

Figure 13. The straight line regression outcomes of hydration heat and the strength of UHSPs at three days of age.

4. Discussion: Comparison of Nano-ZrO_2 and Other Common Nanomaterials

Common nanomaterials added to cement-based materials typically include nano-$CaCO_3$, nano-SiO_2, and nano-TiO_2, etc. The available reports on nano-ZrO_2 are very limited, so we conducted a wide range of experimental studies, including studies on the hydration products, strength, autogenous shrinkage, and hydration heat of UHSP with various contents of nano-ZrO_2. This study is of great significance for filling the gap in the study of cementitious materials with nano-ZrO_2. Firstly, regarding reactivity, Yu et al. [47] reported that through thermogravimetric analysis, nano-SiO_2 can be shown to react with $Ca(OH)_2$ to produce more calcium-silicate-hydrate (C-S-H) gels. In this study, by combining XRD and TG analysis, it was found that nano-ZrO_2 is chemically inert. Secondly, concerning compressive strength, Moro et al. [48] found that nano-TiO_2 was inert but affected the compressive strengths because the CH orientation degree decreased. Similarly, this study found that with a growing amount of nano-ZrO_2, the interior CH orientation amount of the UHSPs decreased. This is crucial for

compressive strength enhancement. Finally, concerning autogenous shrinkage, Li et al. [49] found that UHPC with the addition of nano-$CaCO_3$ had a greater shrinkage. In the present study, the UHSP with nano-ZrO_2 similarly showed an increase in autogenous shrinkage. In addition, the use of internal curing [50] and chemical admixture methods (such as an expansive agent [51] and shrinkage-reducing agent [52]) can be advantageous in terms of reducing autogenous shrinkage, and this will be further investigated in future studies.

In this paper, it was found that nano-ZrO_2 has both positive and negative effects on UHSP. The positive effect was shown to be that the nano-ZrO_2 enhances the compressive strength of UHSP. On the other hand, nano-ZrO_2 has some adverse implications for UHSP. First, the flow of UHSP decreased with the addition of nano-ZrO_2. This factor will create difficulties in the construction of cast-in-place concrete. In addition, the autogenous shrinkage of UHSP increased with the addition of nano-ZrO_2. In future studies, it will be necessary to investigate the method to reduce the autogenous shrinkage of UHSP with nano-ZrO_2. Finally, compared to the cost of cement, nano-ZrO_2 is more expensive. However, it is useful for the production of UHSP, because nano-ZrO_2 can dramatically increase the compressive strength. Based on the study of compressive strength, autogenous shrinkage, and hydration heat, in general, the positive effect concerning the strength improvement of nano-ZrO_2 on UHSP is evident. Therefore, this nanomaterial is viable.

5. Conclusions

By studying the effects of nano-zirconium dioxide on the shrinkage, compressive strength, and hydration heat of UHSPs, the following conclusions were drawn:

1. The flow of UHSPs reduced as the nZr amount increased. The flow values of nZr0, nZr1.5, and nZr3 were 360, 332.5, and 257.5 mm, respectively. With the nZr content increasing, the flow decreased;
2. The nZr increased the heat release of UHSPs. The final heat release values of nZr3, nZr1.5, and nZr0 were 169.58, 164.81, and 163.08 J/g, respectively. Compared with the heat flow of nZr0, the nZr addition increased the height of the main heat flow peak and shortened its appearance time. Therefore, nZr has a physical nucleation effect. The setting time was determined using the isothermal calorimetry method. The setting time was shortened with the addition of nZr to UHSP. This behavior occurs because the addition of nZr provides more nucleation sites for the formation of hydration productions;
3. The nZr increased the total shrinkage of the UHSPs. At 7 days of age, the autogenous shrinkage strain of nZr0, nZr1.5, and nZr3 reached −1158, −1222, and −1739 μm/m, respectively. The entire AS strain was elevated because the nZr amount was elevated. The AS trends of the UHSPs were split into two stages: a stage of variable-temperature and a stage of room-temperature. The split time between the two stages occurred in approximately 1.5 days. In the V stage, the IRH curve peaks of all specimens firstly decreased and then increased. Moreover, in the R stage, the IRH continued to decline. The IRH final values of the UHSPs decreased as the nZr content increased;
4. Regarding the XRD data, new production peaks were not observed, and the peaks of CH did not change significantly. In addition, it was found that the addition of nZr caused a decrease in the degree of internal CH orientation. Regarding the DTA-TG curves, it was found, from the calculation results, that the amount of CH was almost the same as the nZr addition. Therefore, it can be proved that the nZr in this study was chemically inert and did not take part in the cement hydration reaction;
5. There is a linear relationship between the 3-day hydration heat and compressive strength. With the nZr amount increasing, the strength of UHSP at 3 days, 7 days, and 4 weeks all increased. Compared with the 28-day compressive strength of nZr0 (91.9 MPa), the 28-day compressive strength of nZr1.5 (98.8 MPa) and nZr3 (105.0 MPa) increased by 7.5% and 14.27%, respectively.

Author Contributions: Conceptualization, G.-Z.Z. and X.-Y.W.; Data curation, G.-Z.Z. and H.-S.L.; Formal analysis, H.-S.L.; Investigation, G.-Z.Z.; Methodology, X.-Y.W.; Project administration, X.-Y.W.; Visualization,

G.-Z.Z.; Writing—original draft, G.-Z.Z., H.-S.L., and X.-Y.W. All authors have read and agreed to the published version of the manuscript.

Funding: This research was supported by the National Research Foundation of Korea (NRF-2015R1A5A1037548, and NRF-2020R1A2C4002093).

Conflicts of Interest: The authors declare that they have no conflict of interest to declare regarding this work.

References

1. Shi, C.; Wu, Z.; Xiao, J.; Wang, D.; Huang, Z.; Fang, Z. A review on ultra high performance concrete: Part I. Raw materials and mixture design. *Constr. Build. Mater.* **2015**, *101*, 741–751. [CrossRef]
2. Wang, D.; Shi, C.; Wu, Z.; Xiao, J.; Huang, Z.; Fang, Z. A review on ultra high performance concrete: Part II. Hydration, microstructure and properties. *Constr. Build. Mater.* **2015**, *96*, 368–377. [CrossRef]
3. Liu, K.Z.; Yu, R.; Shui, Z.H.; Li, X.S.; Guo, C.; Yu, B.L.; Wu, S. Optimization of autogenous shrinkage and microstructure for Ultra-High Performance Concrete (UHPC) based on appropriate application of porous pumice. *Constr. Build. Mater.* **2019**, *214*, 369–381. [CrossRef]
4. Kodur, V.K.R.; Bhatt, P.P.; Soroushian, P.; Arablouei, A. Temperature and stress development in ultra-high performance concrete during curing. *Constr. Build. Mater.* **2016**, *122*, 63–71. [CrossRef]
5. Ghafari, E.; Costa, H.; Júlio, E.; Portugal, A.; Durães, L. The effect of nanosilica addition on flowability, strength and transport properties of ultra high performance concrete. *Mater. Des.* **2014**, *59*, 1–9. [CrossRef]
6. Chunping, G.; Qiannan, W.; Jintao, L. The effect of nano-TiO_2 on the durability of Ultra-High performance concrete with and without a flexural load. *Ceram. Silik.* **2018**, *62*, 374–381.
7. Gad, M.M.; Rahoma, A.; Al-Thobity, A.M.; ArRejaie, A.S. Influence of incorporation of ZrO_2 nanoparticles on the repair strength of polymethyl methacrylate denture bases. *Int. J. Nanomed.* **2016**, *11*, 5633–5643. [CrossRef]
8. Lu, X.; Xia, Y.; Liu, M.; Qian, Y.; Zhou, X.; Gu, N.; Zhang, F. Improved performance of diatomite-based dental nanocomposite ceramics using layer-by-layer assembly. *Int. J. Nanomed.* **2012**, *7*, 2153–2164.
9. Han, B.; Wang, Z.; Zeng, S.; Zhou, D.; Yu, X.; Cui, X.; Ou, J. Properties and modification mechanisms of nano-zirconia filled reactive powder concrete. *Constr. Build. Mater.* **2017**, *141*, 426–434. [CrossRef]
10. Ruan, Y.; Han, B.; Yu, X.; Li, Z.; Wang, J.; Dong, S.; Ou, J. Mechanical behaviors of nano-zirconia reinforced reactive powder concrete under compression and flexure. *Constr. Build. Mater.* **2018**, *162*, 663–673. [CrossRef]
11. Trejo-Arroyo, D.; Acosta, K.; Cruz, J.; Valenzuela-Muñiz, A.; Vega-Azamar, R.; Jiménez, L. Influence of ZrO_2 Nanoparticles on the Microstructural Development of Cement Mortars with Limestone Aggregates. *Appl. Sci.* **2019**, *9*, 598. [CrossRef]
12. Yuan, H.; Shi, Y.; Xu, Z.; Lu, C.; Ni, Y.; Lan, X. Influence of nano-ZrO_2 on the mechanical and thermal properties of high temperature cementitious thermal energy storage materials. *Constr. Build. Mater.* **2013**, *48*, 6–10. [CrossRef]
13. Cao, M.; Ming, X.; He, K.; Li, L.; Shen, S. Effect of Macro-, Micro- and Nano-Calcium Carbonate on Properties of Cementitious Composites—A Review. *Materials* **2019**, *12*, 781. [CrossRef] [PubMed]
14. ASTM International. *Standard Test Method for Flow of Hydraulic Cement Mortar*; American Society for Testing and Materials: West Conshohocken, PA, USA, 2015; p. 3.
15. Hu, J.; Ge, Z.; Wang, K. Influence of cement fineness and water-to-cement ratio on mortar early-age heat of hydration and set times. *Constr. Build. Mater.* **2014**, *50*, 657–663. [CrossRef]
16. Jensen, O.M.; Lura, P.; Goodwin, F.; Bentz, D.; Hooton, D.; Kovler, K.; Weiss, J. *Standard Test Method for Autogenous Strain of Cement Paste and Mortar*; ASTM International: West Conshohocken, PA, USA, 2016.
17. Active Standard ASTM C349. *Standard Test Method for Compressive Strength of HydraulicCement Mortars (Using Portions of Prisms Broken in Flexure)*; ASTM International: West Conshohocken, PA, USA, 2018.
18. Senff, L.; Hotza, D.; Lucas, S.; Ferreira, V.M.; Labrincha, J.A. Effect of nano-SiO_2 and nano-TiO_2 addition on the rheological behavior and the hardened properties of cement mortars. *Mater. Sci. Eng. A* **2012**, *532*, 354–361. [CrossRef]
19. Sakir, S.; Raman, S.N.; Safiuddin, M.; Kaish, A.B.M.A.; Rahman, K.T.; Mutalib, A.A. Effects of Nano-Materials on Key Properties of Cementitious Composites: A Review. *Electron. J. Struct. Eng.* **2018**, *17*, 1–12.

20. Korayem, A.H.; Tourani, N.; Zakertabrizi, M.; Sabziparvar, A.M.; Duan, W.H. A review of dispersion of nanoparticles in cementitious matrices: Nanoparticle geometry perspective. *Constr. Build. Mater.* **2017**, *153*, 346–357. [CrossRef]
21. Daimon, M.; Roy, D.M. Rheological properties of cement mixes: II. Zeta potential and preliminary viscosity studies. *Cem. Concr. Res.* **1979**, *9*, 103–110. [CrossRef]
22. Cristiano, E.; Hu, Y.-J.; Siegfried, M.; Kaplan, D.; Nitsche, H. A Comparison of Point of Zero Charge Measurement Methodology. *Clays Clay Miner.* **2011**, *59*, 107–115. [CrossRef]
23. Li, L.; Sagüés, A.A.; Poor, N. In situ leaching investigation of pH and nitrite concentration in concrete pore solution. *Cem. Concr. Res.* **1999**, *29*, 315–321. [CrossRef]
24. Ersoy, B.; Dikmen, S.; Uygunoğlu, T.; İçduygu, M.G.; Kavas, T.; Olgun, A. Effect of mixing water types on the time-dependent zeta potential of Portland cement paste. *Sci. Eng. Compos. Mater.* **2013**, *20*, 285–292. [CrossRef]
25. Rong, Z.; Sun, W.; Xiao, H.; Jiang, G. Effects of nano-SiO_2 particles on the mechanical and microstructural properties of ultra-high performance cementitious composites. *Cem. Concr. Compos.* **2015**, *56*, 25–31. [CrossRef]
26. Meng, W.; Khayat, K.H. Effect of graphite nanoplatelets and carbon nanofibers on rheology, hydration, shrinkage, mechanical properties, and microstructure of UHPC. *Cem. Concr. Res.* **2018**, *105*, 64–71. [CrossRef]
27. Mohseni, E.; Naseri, F.; Amjadi, R.; Khotbehsara, M.M.; Ranjbar, M.M. Microstructure and durability properties of cement mortars containing nano-TiO_2 and rice husk ash. *Constr. Build. Mater.* **2016**, *114*, 656–664. [CrossRef]
28. Polat, R.; Demirboğa, R.; Karagöl, F. The effect of nano-MgO on the setting time, autogenous shrinkage, microstructure and mechanical properties of high performance cement paste and mortar. *Constr. Build. Mater.* **2017**, *156*, 208–218. [CrossRef]
29. Yoo, D.-Y.; Park, J.-J.; Kim, S.-W.; Yoon, Y.-S. Early age setting, shrinkage and tensile characteristics of ultra high performance fiber reinforced concrete. *Constr. Build. Mater.* **2013**, *41*, 427–438. [CrossRef]
30. Zhang, M.-H.; Sisomphon, K.; Ng, T.S.; Sun, D.J. Effect of superplasticizers on workability retention and initial setting time of cement pastes. *Constr. Build. Mater.* **2010**, *24*, 1700–1707. [CrossRef]
31. Jansen, D.; Neubauer, J.; Goetz-Neunhoeffer, F.; Haerzschel, R.; Hergeth, W.-D. Change in reaction kinetics of a Portland cement caused by asuperplasticizer—Calculation of heatflow curves from XRD data. *Cem. Concr. Res.* **2012**, *42*, 327–332. [CrossRef]
32. Chen, Y.; Deng, Y.-F.; Li, M.-Q. Influence of Nano-SiO_2 on the Consistency, Setting Time, Early-Age Strength, and Shrinkage of Composite Cement Pastes. *Adv. Mater. Sci. Eng.* **2016**, *2016*, 5283706. [CrossRef]
33. Tafesse, M.; Kim, H.-K. The role of carbon nanotube on hydration kinetics and shrinkage of cement composite. *Compos. Part B Eng.* **2019**, *169*, 55–64. [CrossRef]
34. Bentz, D.P.; Geiker, M.R.; Hansen, K.K. Shrinkage-reducing admixtures and early-age desiccation in cement pastes and mortars. *Cem. Concr. Res.* **2001**, *31*, 11. [CrossRef]
35. Qing, Y.; Zenan, Z.; Deyu, K.; Rongshen, C. Influence of nano-SiO_2 addition on properties of hardened cement paste as compared with silica fume. *Constr. Build. Mater.* **2007**, *21*, 7. [CrossRef]
36. Han, B.; Li, Z.; Zhang, L.; Zeng, S.; Yu, X.; Han, B.; Ou, J. Reactive powder concrete reinforced with nano SiO_2-coated TiO_2. *Constr. Build. Mater.* **2017**, *148*, 104–112. [CrossRef]
37. Zhang, Z.; Zhang, B.; Yan, P. Comparative study of effect of raw and densified silica fume in the paste, mortar and concrete. *Constr. Build. Mater.* **2016**, *105*, 82–93. [CrossRef]
38. Meng, T.; Yu, Y.; Qian, X.; Zhan, S.; Qian, K. Effect of nano-TiO2 on the mechanical properties of cement mortar. *Constr. Build. Mater.* **2012**, *29*, 241–245. [CrossRef]
39. Scrivener, K.; Snellings, R.; Lothenbach, B. *A Practical Guide to Microstructural Analysis of Cementitious Materials*; CRC Press: Boca Raton, FL, USA, 2016.
40. Dweck, J.; Buchler, P.M.; Coelho, A.C.V.; Cartledge, F.K. Hydration of a Portland cement blendedwith calcium carbonat. *Thermochim. Acta* **2000**, *346*, 105–113. [CrossRef]
41. Kim, T.; Olek, J. Effects of Sample Preparation and Interpretation of Thermogravimetric Curves on Calcium Hydroxide in Hydrated Pastes and Mortars. *Transp. Res. Rec. J. Transp. Res. Board* **2012**, *2290*, 10–18. [CrossRef]
42. Monteagudo, S.M.; Moragues, A.; Gálvez, J.C.; Casati, M.J.; Reyes, E. The degree of hydration assessment of blended cement pastes by differential thermal and thermogravimetric analysis. Morphological evolution of the solid phases. *Thermochim. Acta* **2014**, *592*, 37–51. [CrossRef]

43. Chithra, S.; Senthil Kumar, S.R.R.; Chinnaraju, K. The effect of Colloidal Nano-silica on workability, mechanical and durability properties of High Performance Concrete with Copper slag as partial fine aggregate. *Constr. Build. Mater.* **2016**, *113*, 794–804. [CrossRef]
44. Ghafari, E.; Arezoumandi, M.; Costa, H.; Júlio, E. Influence of nano-silica addition on durability of UHPC. *Constr. Build. Mater.* **2015**, *94*, 181–188. [CrossRef]
45. Aïtcin, P.-C.; Flatt, R. *Science and Technology of Concrete Admixtures*; Woodhead Publishing: Cambridge, UK, 2016; p. 666.
46. Loukili, A.; Khelidj, A.; Richard, P. Hydration kinetics, change of relative humidity, and autogenous shrinkage of ultra-high-strength concrete. *Cem. Concr. Res.* **1999**, *29*, 577–584. [CrossRef]
47. Yu, R.; Spiesz, P.; Brouwers, H.J.H. Effect of nano-silica on the hydration and microstructure development of Ultra-High Performance Concrete (UHPC) with a low binder amount. *Constr. Build. Mater.* **2014**, *65*, 140–150. [CrossRef]
48. Moro, C.; El Fil, H.; Francioso, V.; Velay-Lizancos, M. Influence of water-to-binder ratio on the optimum percentage of nano-TiO2 addition in terms of compressive strength of mortars: A laboratory and virtual experimental study based on ANN model. *Constr. Build. Mater.* **2020**. [CrossRef]
49. Li, W.; Huang, Z.; Zu, T.; Shi, C.; Duan, W.; Shah, S.P. Influence of Nanolimestone on the Hydration, Mechanical Strength, and Autogenous Shrinkage of Ultrahigh-Performance Concrete. *J. Mater. Civ. Eng.* **2016**, *28*. [CrossRef]
50. Zhang, J.; Wang, Q.; Zhang, J. Shrinkage of internal cured high strength engineered cementitious composite with pre-wetted sand-like zeolite. *Constr. Build. Mater.* **2017**, *134*, 664–672. [CrossRef]
51. Yoo, D.Y.; Kim, S.; Lee, J.Y.; You, I.; Lee, S.J. Implication of calcium sulfoaluminate-based expansive agent on tensile behavior of ultra-high-performance fiber-reinforced concrete. *Constr. Build. Mater.* **2019**, *217*, 679–693. [CrossRef]

52. Yoo, D.-Y.; Banthia, N.; Yoon, Y.-S. Effectiveness of shrinkage-reducing admixture in reducing autogenous shrinkage stress of ultra-high-performance fiber-reinforced concrete. *Cem. Concr. Compos.* **2015**, *64*, 27–36. [CrossRef]